Bidirectional Absorber from Broadband to Narrowband Using Epsilon-Near-Zero material and Plasmonic Structures

Hamideh Kondori, Majid Ghadrdan*, and Mohammad Ali Mansouri-Birjandi

Faculty of Electrical and Computer Engineering, University of Sistan and Baluchestan (USB), Zahedan, Iran

Corresponding author email: Ghadrdan@ece.usb.ac.ir

ABSTRACT—In this study, a bidirectional absorber with broadband and narrowband absorption capabilities is designed and analyzed. The structure consists of two sides: the top side is composed of Au disks and indium tin oxide (ITO) as an epsilon-near-zero (ENZ) material for broadband absorption in the near-infrared region, whereas the bottom side features a simple metal-dielectric-metal configuration for narrowband absorption. Broadband absorption, covering more than 90% of the spectrum within the wavelength range of 1470–2290 nm, results from the coupling of the ENZ modes with the plasmon modes. Narrowband absorption with near-unity efficiency at a wavelength of 1550 nm was achieved because of the localized plasmonic resonances in the Al disk arrays. The numerical simulation results demonstrate that this structure can achieve nearly perfect absorption in both light propagation directions ($+z$ and $-z$) through the optimization of geometric parameters. In addition, this design has potential applications in color filters, energy storage systems, and advanced optical devices.

KEYWORDS: Epsilon-near-zero material, Bidirectional absorber, Broadband, Narrowband, Perfect absorption.

I. INTRODUCTION

The absorption of electromagnetic waves is a critical phenomenon that involves energy conversion upon the interaction of light with a material. This process has applications across various domains, including defense, sensing, imaging, medical treatments, cloaking technologies, and solar energy harvesting [1]-[7].

Metamaterial absorbers have garnered significant attention from researchers owing to their thinness compared to traditional absorbers. Recently, a class of materials known as epsilon-near-zero (ENZ) materials has been identified, characterized by their near-zero permittivity [8]. The frequency at which the real part of permittivity approaches zero is referred to as the ENZ frequency [9]. The region surrounding the ENZ wavelength, where $|\mathrm{Re}\{\varepsilon\}|<1$, is defined as the ENZ region [10], [11]. Owing to their remarkable optical properties, these materials have found many applications in various fields such as switches [12]-[16], optical modulators [17]-[23], isolators [24], sensors [25], absorbers [26]-[31], filters [32], [33], and image resolution [34]. Transparent conducting oxides (TCOs) are the most popular ENZ materials owing to their functional feasibility and unique properties. One of the most widely used TCOs is indium tin oxide (ITO), which has a high electron density in the range of 10^{19} to 10^{21} cm^{-3} [35], [36].

In various research fields, absorbers with either broadband or narrow-band absorption have been developed, depending on the application requirements. These structures play an

important role in various devices, such as thermal emitters [37], [38], color filters [39], and chemical sensing [40], [41]. Recently, perfect absorbers with the ability to achieve broadband and narrowband absorption have opened up new research areas in many fields [42], [43].

A tunable absorber comprising an array of silicon pillars embedded within a Liquid Crystal (LC) layer controlled by graphene electrodes was reported. By altering the applied bias, the orientation of the LC can be adjusted, enabling achievement of the desired absorption peaks [43]. A perfectly tunable absorber was introduced by employing a graphene layer as an optical switch specifically designed for infrared applications [44]. A multilayer absorber with tunable functionality that leverages vanadium dioxide (VO$_2$) as the switching material is presented. The device exhibited broadband absorption in the metallic state of VO$_2$ and narrowband selective absorption in its insulating state [45]. A terahertz absorber capable of switching between four narrow bands and a single broadband absorption mode is introduced. The structure leverages a combination of graphene and VO$_2$, both of which exhibit tunable electrooptical properties. By controlling the phase transition of VO$_2$ and adjusting the Fermi level of graphene, the absorber performance can be switched between different operational states [46]. A combination of cross-patterned graphene and square frames was utilized to achieve wideband and narrowband optical switching. By applying an electric field to the graphene layer and adjusting its relaxation time, the desired wideband and narrowband absorption characteristics were achieved [47].

Although it is possible to achieve both broadband and narrowband absorption in a single-sided structure, this approach increases the device complexity. Moreover, a portion of the broadband absorption bandwidth is wasted

to meet both the broadband and narrowband absorption requirements [48].

In this study, we designed a bidirectional absorber that enables broadband and narrowband absorption without any external mechanisms. The use of ITO in the top layer, which functions as an ENZ material in the near-infrared region, provides broadband absorption through the excitation of ENZ modes and their coupling to plasmon modes.

The coupling between ENZ modes in the ITO layer and plasmonic modes in the gold (Au) disks plays a critical role in achieving high absorption efficiency. This interaction markedly enhances the local electric field and broadens the spectral bandwidth of light absorption. For the bottom layer, which enables narrowband absorption, a conventional metal–dielectric–metal configuration is employed, where localized plasmonic resonances are supported by Al disk arrays.

The proposed bidirectional absorber addresses the challenges of design complexity and bandwidth reduction when switching from broadband to narrowband states. This structure has potential applications in energy storage systems, color filters, sensors, and optoelectronic devices.

In the top layer, the generation of plasmonic modes is primarily facilitated by the Au disks, which induce collective oscillations of free electrons at the metal–dielectric interface, resulting in localized plasmonic resonances. Conversely, ENZ modes are excited within the ITO layer. The coupling between these two modes-ENZ in ITO and plasmonic in Au substantially enhances absorption by intensifying the local electric field and broadening the spectral response.
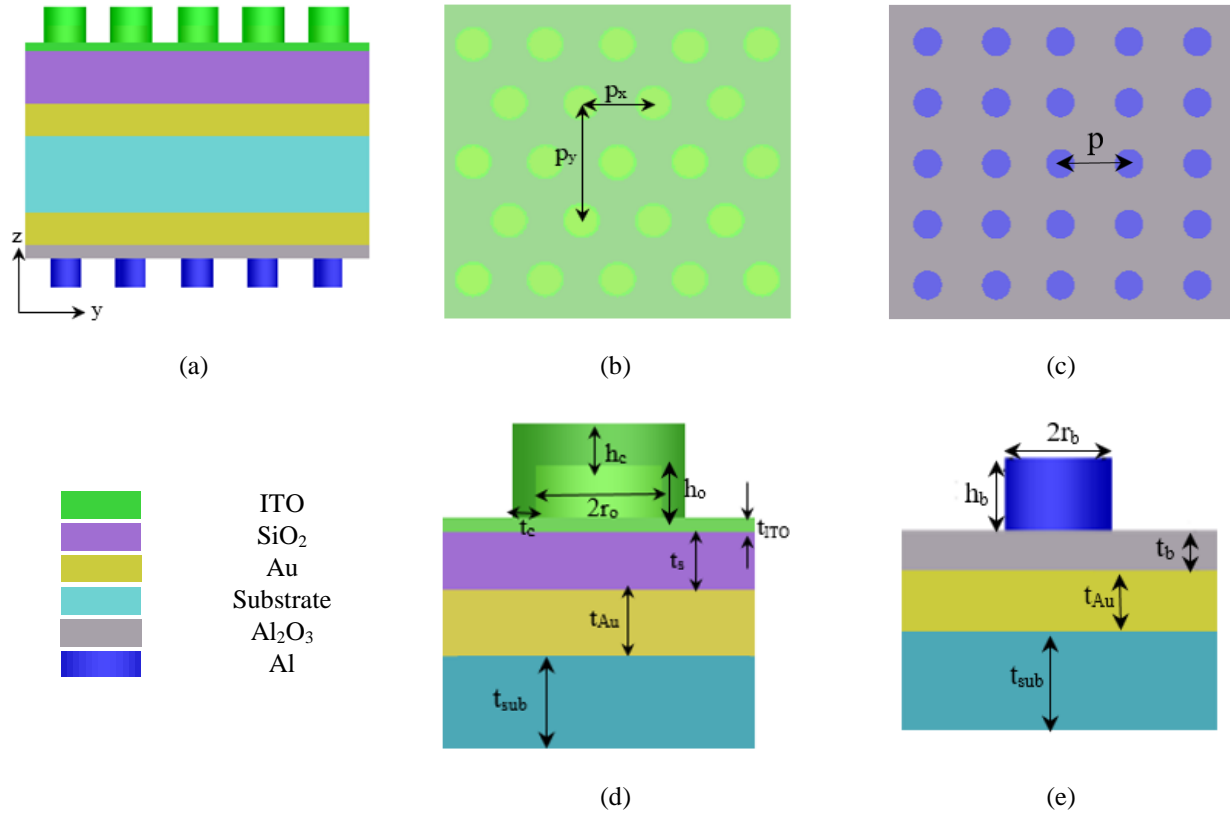
Fig. 1. (a) The cross-section view of the bidirectional perfect absorber. (b)-(c) Top views of the layers in the (+z) and (−z) directions, respectively. (d)-(e) Parameter representations for the upper section and lower section, respectively.

II. MODELS AND METHODS

Figure 1 illustrates the proposed design of a bidirectional switchable perfect absorber. The structure exploits the simultaneous excitation of ENZ modes in the ITO layer and plasmonic modes in the Au disks to achieve tunable and efficient light absorption. The top side of the absorber comprises triangularly arranged Au disks, a SiO$_2$ spacer, and a thick Au plate that functions as a ground plane. To achieve broadband absorption, the ENZ material was incorporated into the structure. For excitation of the ENZ mode, the film thickness must be much smaller than the critical thickness of $\lambda_{ENZ}/50$, where λ_{ENZ} is the wavelength at which the real part of the dielectric permittivity reaches zero [49]. A 12 nm ultra-thin coating of ITO, exhibiting ENZ properties at a wavelength of 1550 nm, was placed between the Au array and spacer. Additionally, ITO coatings covered the sides and tops of the disks with thicknesses of t_c=20 nm and h_c = 80 nm, respectively. This

further enhances the absorption, resulting in robust and efficient performance.

The lower absorber segment employed a similar metal-dielectric-metal configuration, and consisted of a square periodic array of Al disks placed on an Al$_2$O$_3$ dielectric layer. This design is supported by a thick Au ground plane mounted on a glass substrate. In this model, the structural parameters are optimized to achieve perfect absorption. The optimized dimensions included the radius of the Au disks (r_o) of 185 nm and their height (h_o) of 50 nm. The radius and height of the Al disks were determined as r_b=153 nm and h_b=30 nm, respectively. Furthermore, the thickness of the ground Au layer was set to t_{Au}=190 nm on both sides to ensure effective absorption in both the directions. The spacer layer thickness was investigated in both directions and the optimal dimensions were t_s=185 nm for SiO$_2$ and t_b=28 nm for Al$_2$O$_3$. For the top of the absorber (+z direction), the periodicity in the x and y

directions was 750 nm and 1275 nm, respectively. In addition, for the Al square arrays in the x-direction, the periodicity was 800 nm.

Appropriate selection of the lattice periodicities, disk dimensions, and ITO coating thickness is critical to precluding inter-element filling and sustaining robust absorption performance.

In the absorber design, the absorption coefficient (*A*) is mathematically defined as a function of the reflection (*R*) and transmission (*T*) through the relationship *A=1−R−T*. In this study, the transmission was completely eliminated because the optically thick Au layer effectively prevented light from propagating through the structure. Consequently, the absorption is primarily determined by the reflection properties.

To accurately simulate the interaction of a propagating plane electromagnetic wave with the absorber, periodic boundary conditions were applied along the x and y directions, while a perfect matching layer (PML) was utilized along the z direction to effectively suppress unwanted boundary reflections. The reflectivity of the device in both forward and backward directions is calculated using the finite-difference time-domain (FDTD) method under plane wave illumination, from which the absorption spectrum is subsequently derived. The optical constants for SiO_2, Al_2O_3, Au, and Al were sourced from the Palik standard database [50] to ensure the reliability of the input parameters. The optical response of the ITO, which is essential for identifying the ENZ region, was derived using the Drude model. This model is described by the following equation [51]:

$$\varepsilon_{ITO}(\omega) = \varepsilon_\infty - \frac{\omega_p^2}{\omega^2 + i\Gamma\omega} \qquad (1)$$

where ε_∞ is the high-frequency dielectric constant, ω_p is the plasma frequency, Γ is the electron attenuation rate, and ω is the angular frequency of the incident wave. Parameters ω_p and Γ were determined using the following equations:

$$\omega_p^2 = \frac{ne^2}{\varepsilon_0 m^*}, \qquad (2)$$

$$\Gamma = \frac{e}{m^*\mu}, \qquad (3)$$

where ε_0 is the permittivity of free space, e is the electron charge, m^* is the electron effective mass, *n* is the free carrier density in ITO, and μ is the electron mobility. These parameters enable precise characterization of ITO's dispersive properties within the ENZ regime. To achieve ENZ properties in ITO at a wavelength of 1550 nm, specific material parameters were utilized, as outlined in [52]:

μ=38 cm^2/V.s, ε_∞=3.49, n=7.5×1019 cm^{-3}, ω_p=8.24×10^{14} rad/s, and m^*=0.35m_0 (m_0 is the mass of the electron in free space). These parameters enabled ITO to exhibit ENZ characteristics by fine-tuning the carrier density (*n*) within the material. This tunability is essential for ENZ applications and can be accurately controlled during material fabrication using techniques such as atomic layer deposition, sputtering, and other deposition methods [53]. Such control over the ENZ is critical for designing devices in fields such as nanophotonics and metamaterials, where specific optical responses are required at telecommunication wavelengths. Moreover, by tailoring these parameters, ITO-based devices can achieve enhanced light-matter interactions. In this regard, the relative permittivity curve of ITO, as shown in Fig. 2, indicates that λ_{ENZ} is 1550 nm.

The optical response of the structure was characterized by its absorption behavior under normal light incidence, as shown in Fig. 3. The results indicate that the structure exhibits near-unity absorption, with reflectance approaching zero in both the forward and backward directions. This high absorption in both directions demonstrates the high efficiency of the structure in trapping and utilizing the incident light. Under forward incidence, the confinement of the electric field within the ENZ layer significantly enhances the interaction between the electromagnetic waves and the material. This confinement enables coupling between the excited ENZ and the plasmon

modes. The coupling effect amplifies the local electric field intensity and broadens the spectral range of light absorption. Consequently, this interaction leads to a substantial increase in light absorption over a range wider than the typical bandwidth, thereby improving the optical response of the system.
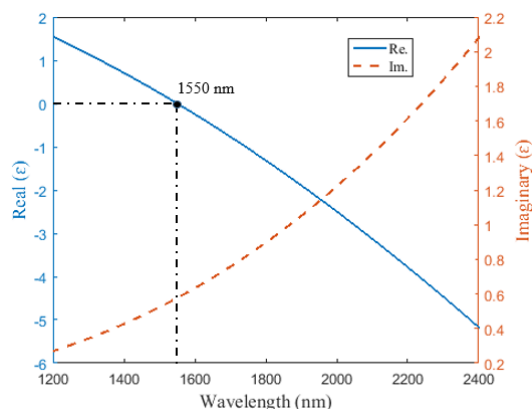

Fig. 2. Permittivity spectrum of ITO

As is evident from Fig. 3(a), the structure achieves absorption levels exceeding 90% across a broad wavelength range from 1470 to 2290 nm. This behavior highlights the potential of the structure as an effective broadband absorber suitable for various applications requiring high-efficiency light capture, such as energy harvesting, photodetectors, and thermal emission control. As shown in Fig. 3(b), under backward incidence, the structure maintains its remarkable optical performance. Specifically, near-unity absorption was observed at a wavelength of 1550 nm, indicating a pronounced resonance. The high absorptivity at this resonance wavelength highlights the suitability of the structure for applications where precise spectral selectivity is critical, such as optical filters, sensors, or communication systems. Furthermore, the minimal reflectance in both directions confirms efficient impedance matching between the structure and the surrounding medium, which facilitates maximum light absorption. Therefore, the device enables simultaneous access to both broadband and narrowband absorption states, depending on specific application requirements. Additionally, it can function as a switch between two distinct absorption conditions.
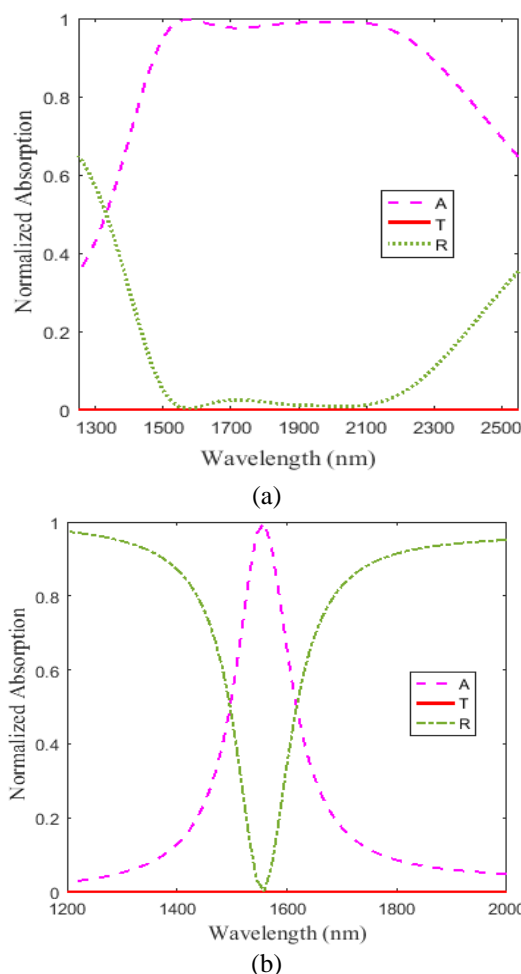

(a)

(b)

Fig. 3. Simulated absorptivity response of the bidirectional absorber for a normally incident plane wave propagating in the (a) forward and (b) backward directions.

III. RESULTS AND DISCUSSION

The thickness of the SiO_2 layer, which functions as a spacer, plays a crucial role in determining the absorption rate of the system. Figure 4 illustrates the variations in the absorption rates corresponding to the different spacer thicknesses. The peak I in the absorption spectrum, occurring near the ENZ wavelength, was attributed to the ENZ mode, while the peak II was attributed to the plasmon mode. When the spacer layer is excessively thick, the interaction between these two modes–the ENZ mode and plasmon mode - is significantly weakened owing to the reduced spatial overlap of their electromagnetic fields. This weak coupling led to a decrease in absorption efficiency. In contrast, with an excessive reduction in the thickness of the SiO_2 layer, the spatial overlap between the ENZ and plasmon modes increased, thereby enhancing the

coupling strength between them. This strong coupling results in the emergence of two distinct peaks in the absorption spectrum. The interplay between spacer thickness, coupling strength, and absorption behavior highlights the importance of precise spacer design for optimizing the performance of plasmonic or photonic devices.
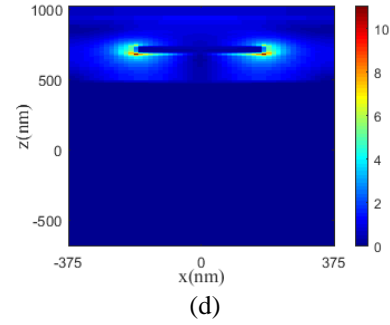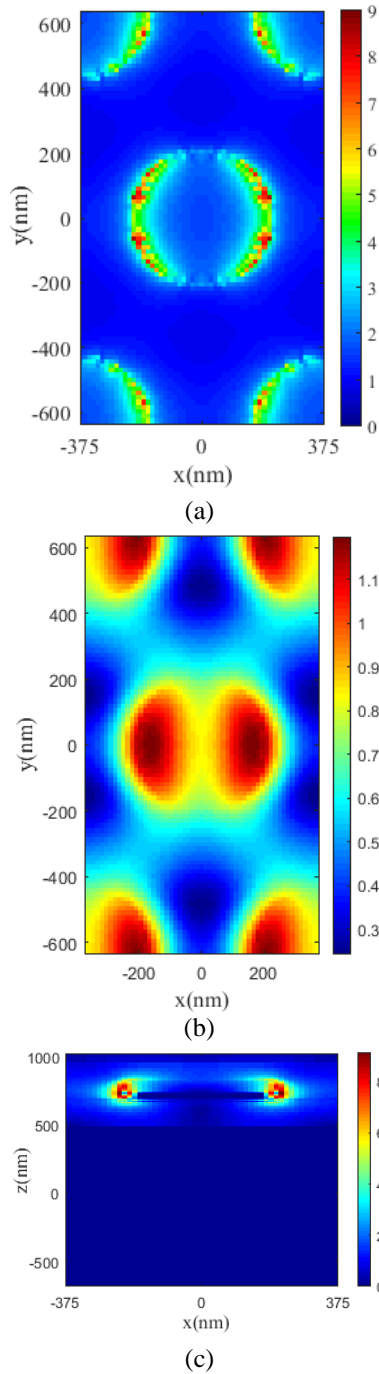

(a)

(b)

(c)

(d)

Fig. 5. Electric field intensity distributions corresponding to the absorption peaks at 1900 nm (a and c) and 1300 nm (b and d): (a)–(b) in the x-y plane, and (c)–(d) in the x-z plane.

To demonstrate the effect of ITO on the bandwidth, the electric and magnetic field distributions at 1900 and 1300 nm, corresponding to wavelengths inside and outside the absorption band, respectively, were simulated and are presented in Fig. 5. As observed in Figs. 5(a) and (c), at the wavelength of 1900 nm, the electric field is strongly confined within the ENZ layers, leading to enhanced optical absorption over a broad bandwidth owing to excitation of the ENZ mode. In contrast, at the wavelength of 1300 nm, the ENZ modes could not be effectively
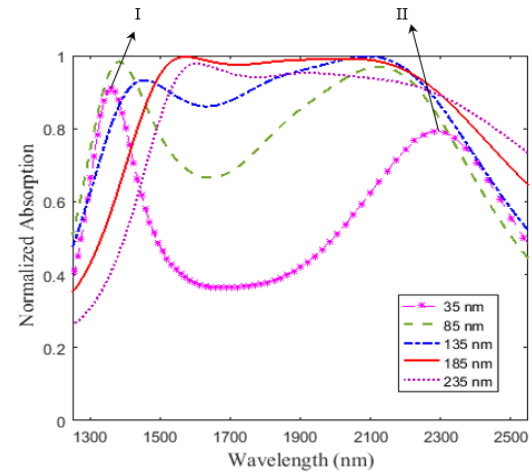

Fig. 4. Simulated absorptivity for various thicknesses of the SiO$_2$ layer.

excited, limiting the confinement of the electric field within the ITO layer. Consequently, only a minimal penetration of the electric field into the adjacent SiO$_2$ dielectric layer was observed. This weak interaction restricts optical absorption at 1300 nm (Figs. 5(b) and (d)).

Therefore, the excitation of ENZ modes within the ITO layer and their coupling with plasmonic modes result in broadband optical absorption.

The bandwidth and absorption peak could be tuned by altering the geometric parameters of the designed device. To determine the optimal value for each parameter, a numerical investigation was performed in which the effect of one parameter was evaluated while keeping the other parameters constant. Achieving the maximum absorption peak value and broad bandwidth necessitates a tradeoff between these two characteristics, ensuring that an optimal balance is chosen.

Figure 6(a) illustrates the effect of varying the Au disk radius in the range 145–195 nm in increments of 10 nm. In the initial stages of increasing the disk radius, the stronger coupling between the disks and ITO enhanced the absorption intensity at peak II. However, beyond approximately 165 nm, the disk distances become sufficiently small such that plasmonic modes exhibit significant overlap, leading to the weakening of the effective coupling and a subsequent reduction in absorption. As the radius increased and the disk gaps decreased, the plasmonic modes in the gap region abnormally intensified, resulting in a reduction in the plasmonic resonance energy and a redshift in the resonance wavelength. In contrast, peak I, associated with the ENZ modes, continuously increased as the enlargement of the disk radius enhanced the coupling between the plasmonic and ENZ modes, thereby strengthening the light absorption in this mode. Furthermore, because the ENZ mode is primarily governed by the dielectric properties of ITO rather than its geometrical dimensions, no significant shift in the peak I wavelength was observed. Ultimately, considering the balance between maximum absorption and bandwidth, an optimal radius of 185 nm was selected, as it maintains a high absorption intensity while maintaining the bandwidth reduction within an acceptable range.

Next, simulations were conducted to determine the optimal height of the Au disks with values

of 30, 40, 50, 60, 70, and 80 nm. As illustrated in Fig. 6(b), increasing the disk height has different effects on the plasmonic and ENZ modes. Peak II exhibited a reduction in the absorption intensity, a shift toward shorter wavelengths (blue shift), and a decrease in the bandwidth as the height increased. In fact, increasing the height enhances ohmic losses, reduces the surface field intensity, and weakens plasmonic coupling with the ITO layer, leading to a decrease in the absorption of the plasmonic peak. Moreover, as the height increased and the concentration of electromagnetic fields at the surface decreased, the oscillation rate of surface charges increased, resulting in a higher resonance frequency and, consequently, a blue shift of peak II. Conversely, peak I remains at a constant wavelength, whereas its absorption intensity increases. This phenomenon occurs because increasing the height enhances the coupling between the plasmonic and ENZ modes, increases the contact area between the disk and ITO layer, and reduces the energy leakage. As a result, more electromagnetic energy is confined within the ITO layer, leading to a higher absorption in this mode. In addition, because the ENZ mode is primarily governed by the intrinsic properties of ITO, increasing the height induces only a minor change, causing a slight redshift. Among the investigated heights, 50 nm provided the most uniform absorption across the entire spectrum. This balance establishes an optimal point between the absorption intensity, bandwidth, and spectral position of resonance peaks. Therefore, an Au disk height of 50 nm was selected as the optimal value.

In subsequent simulations, the optimization of the ITO coating on the sidewalls and top surface of the metallic disks was investigated. Initially, the optimal thickness of the ITO coating on the sidewalls of the disks was determined (Fig. 7(a)). A reference case with no coating was considered, followed by a variation in the thickness from 10 to 50 nm in steps of 10 nm. The results indicated that increasing the thickness led to a broader absorption bandwidth but a reduction in the absorption intensity.
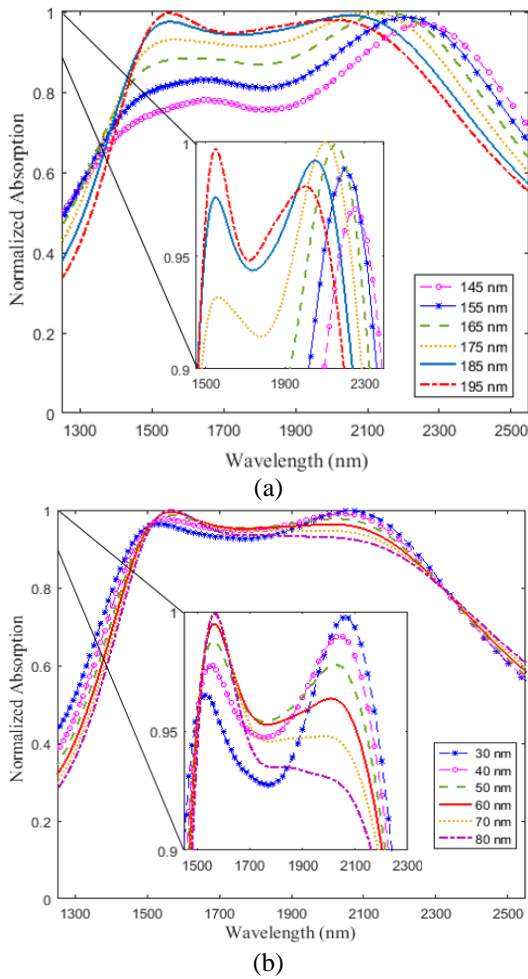
Fig. 6. Absorption spectrum as a function of Au disks (a) radius, (b) height.

reduction in the resonance wavelength. Under these conditions, a thickness of 20 nm yielded favorable results.

For the top ITO coating of the disks, the absence of ITO and coatings with thicknesses of 60, 70, 80, 90, and 100 nm were considered, and the results are presented in Fig. 7(b). At higher thicknesses, the ITO layer moves away from the ENZ regime and begins to exhibit the behavior characteristics of a conventional dielectric material. This change directly influenced the resonance peaks.
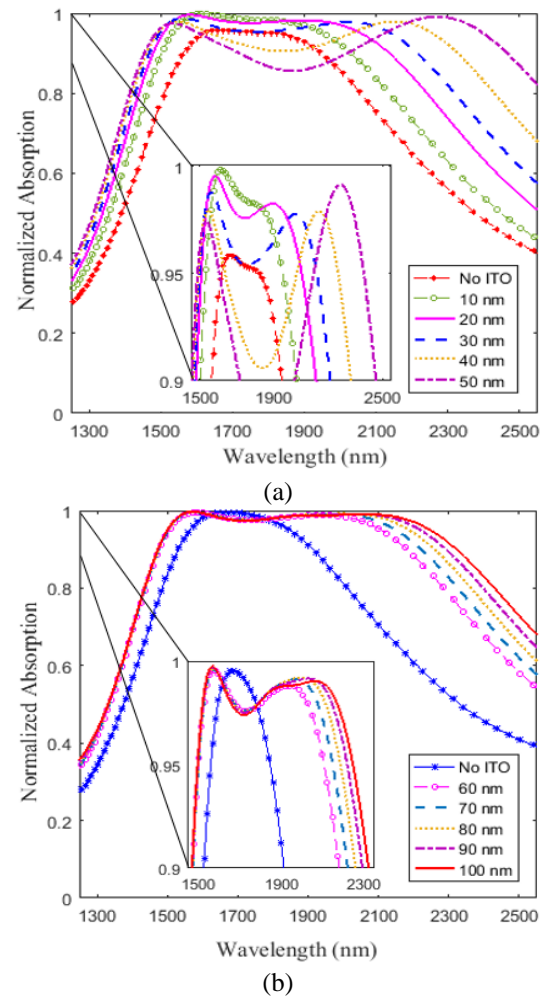

Fig. 7. Variations in absorption rate with (a) changes in the ITO coating thickness on the sidewalls of Au disks and (b) changes in the ITO coating thickness on the top of Au disks.

The oscillatory behavior in the absorption of peak II arises because of the interference of the plasmonic modes, changes in impedance matching, and variations in the coupling between the plasmonic and ENZ modes. Furthermore, the presence of ITO slows the propagation of the electric field within the material, inducing a phase delay in the plasmonic mode and shifting the absorption peak toward longer wavelengths. For peak I, adding an ITO layer and increasing its thickness to 10 nm reduced reflection, enhanced impedance matching, increased field confinement in the ENZ region, and strengthened the coupling between the plasmonic and ENZ modes, thereby improving the absorption. However, at greater thicknesses, the resonance is weak, leading to a reduction in absorption. In addition, as the ITO thickness increased, the effective refractive index increased slightly, resulting in a minor increase in the resonance frequency and a slight

In Peak II, increasing the ITO thickness to 80 nm enhanced the overlap between the electric field and the plasmonic modes. This stronger coupling improves the light absorption and increases the peak intensity. However, for thicknesses exceeding 80 nm, the electric field

120

became more widely distributed within the ITO layer and moved further away from the Au disk surface. This reduced field confinement near the Au disks results in a lower absorption intensity and a redshift in the resonance wavelength. In Peak I, introducing an ITO layer with a thickness below the critical threshold optimized the impedance matching between air and the structure, leading to reduced reflection and enhanced absorption. For thicknesses greater than the critical value, the electric field is no longer confined solely near the Au disk surface but is instead distributed over a larger volume within the ITO layer. Nevertheless, because the overall field strength remained nearly constant, the absorption intensity exhibited negligible variation. Under these conditions, the optimal ITO thickness of 80 nm was selected to achieve the highest absorption efficiency.

Parameter optimization was conducted when the light was incident on the device in the backward direction. In the first stage, the radius of the Al disks was optimized. To determine the optimal value, a radius in the range of 125–175 nm was considered with steps of 10 nm. As illustrated in Fig. 8(a), increasing the radius of the Al disks in the periodic structure led to a redshift in the absorption peak, while the absorption magnitude remained nearly constant. This redshift is attributed to the capacitance enhancement between the disks, reduction in the restoring force of plasmonic oscillations, and enhancement of the effective optical path in the structure. As the disk radius increased, the surface charge density decreased, leading to a weaker electrostatic force that restored the oscillating electrons. Consequently, the resonance frequency decreases, shifting the absorption peak to longer wavelengths. Meanwhile, the absorption level remained unchanged because the increase in the disk surface area compensated for the reduction in the charge density, thereby preventing a significant alteration in the coupling intensity between the plasmonic modes and incident light. According to the obtained results, the wavelength of 1550 nm lies between the absorption peaks corresponding to radii of 145 and 155 nm. To

determine the radius at which resonance occurred at 1550 nm, additional simulations with smaller steps within this range were performed. As shown in Fig. 8(b), the radius at which absorption occurred at the target wavelength was determined to be approximately 153 nm.
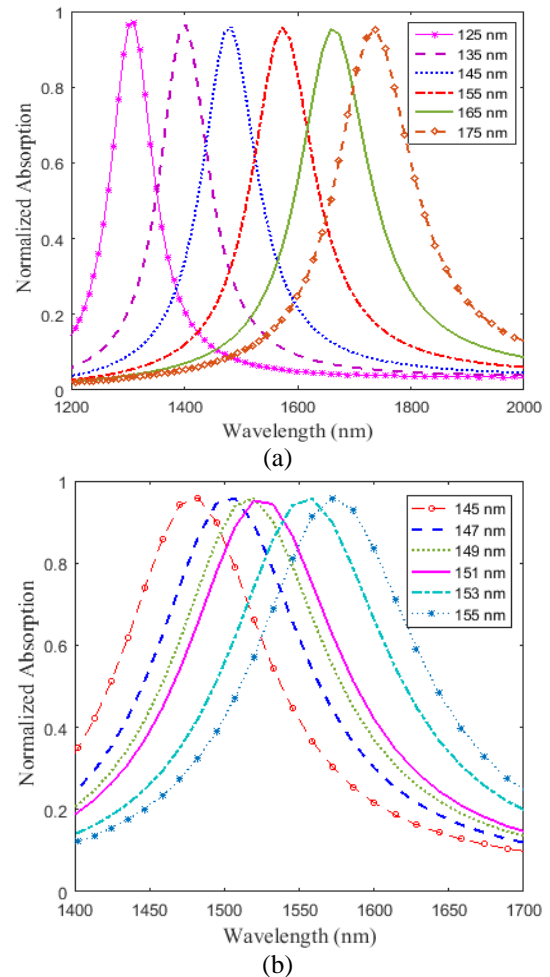

(a)

(b)

Fig. 8 (a) Absorption spectra based on variations in the radius of Al disks, (b) Absorption curve with higher precision in radius variations of Al disks for a more detailed analysis of changes.

In Fig. 9, the effect of the Al disk height on the narrowband absorption is investigated for heights of 20, 30, 40, 50, and 60 nm. The observed variations indicated that the absorption peak initially increased from 20 to 30 nm and subsequently exhibited a decreasing trend. The initial enhancement in absorption up to a height of 30 nm is attributed to the strengthening of plasmonic mode coupling, whereas the reduction in absorption at greater heights is associated with scattering effects, reduced field confinement, and the weakening

of the effective coupling between plasmonic modes and incident light. Accordingly, the optimal height was determined as 30 nm, which represents the maximum absorption level.

Finally, the optimal thickness of the Al_2O_3 dielectric layer (t_b) is determined. Simulations were conducted for dimensions ranging from 20 to 36 nm with 4 nm increments. As illustrated in Fig. 10, at lower thicknesses, the strong coupling between the disks and ground plane enhances the absorption peak. As the thickness increased, plasmonic coupling weakened, leading to a reduction in the peak absorption intensity. As the thickness increased, the capacitance between the disks and the backplane decreased. This reduction in capacitance leads to an increase in the resonance frequency, resulting in a blue shift of the absorption peak toward shorter wavelengths. The optimal thickness of t_b=28 nm resulted in the highest absorption at the target wavelength.
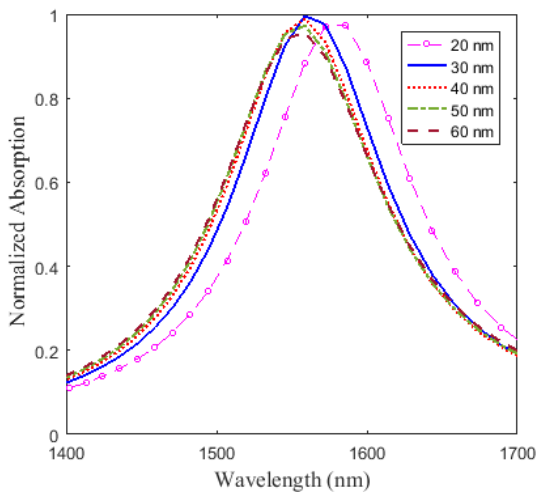

Fig. 9. Influence Al disks height on narrowband absorption.

The performance of the proposed structure in this study was compared with that of previous investigations that implemented various absorption conditions within a single device. As shown in Table 1, our absorber exhibits significant differences from those reported in previous studies in terms of the absorption mechanism, materials used, switching capability, and absorption directionality.

In most previous studies, external switching mechanisms, such as phase-change materials (VO_2) or tuning of the Fermi level of graphene, have been employed to control absorption. However, in this study, an external mechanism was not used to achieve the desired absorption characteristics. Furthermore, ENZ materials with exceptional properties were incorporated to achieve broadband absorption. One of the most critical differences between this study and previous studies is the direction of absorption. Although most prior studies have been limited to unidirectional absorption, the proposed structure in this research is capable of absorbing light in both the +z and −z directions, thus enhancing its flexibility for practical applications. Overall, by utilizing a simple structural design and enabling bidirectional broadband and narrowband absorption without an external mechanism using an ENZ material, this study demonstrates superior performance compared with many previous investigations. The proposed absorber presents an efficient solution for various absorption applications over a wide frequency range.

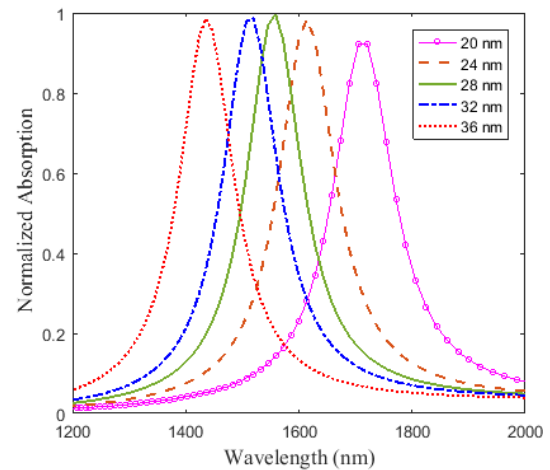Fig. 10. Effect of Al_2O_3 thickness variation on the absorption spectrum.

IV. CONCLUSION

In this study, a bidirectional absorber with broadband and narrowband absorption capabilities is designed and analyzed. Numerical simulation results demonstrated that the combination of plasmon modes with epsilon-near-zero (ENZ) modes in the top side and localized plasmonic resonances in the bottom side significantly enhanced the light

absorption efficiency. The incorporation of indium tin oxide (ITO) into the device improves broadband absorption in the near-infrared region, whereas the Al disk array described in the bottom side ensures precise narrowband absorption. Through optimization of the geometric parameters, the structure achieves near-perfect optical absorption in both

directions of light incidence. This absorber shows great potential for applications in photovoltaic systems, optical filters, advanced sensors, thermal emission control, and optoelectronic devices, serving as a reference for the development of multifunctional optical absorbers in advanced photonic technologies.

Table **1.** Comparison of performance of the proposed absorber compared to other absorbers.

Ref.	Direction of Absorption	Absorption Capability	Switching Mechanism	ENZ Material Utilization in Absorption	Absorption Bandwidth	Absorption Amplitude
[45]	Unidirectional	broadband and narrowband Switchable	VO$_2$ (Phase Change	No	0.393-0.897 THz 0.677 THz	>90% ≈100%
[47]	Unidirectional	broadband and narrowband Switchable	Fermi level of Graphene	No	1.27-2.16 THz 1.72 THz	>90% >99%
[54]	Unidirectional	broadband and narrowband Switchable	VO$_2$ (Phase Change)	No	2.6-6.28 THz 7.77 THz	>90% 99.99%
[55]	Unidirectional	dual-broadband switchable	VO$_2$ (Phase Change) & Graphene (Fermi level)	No	1.10–2.30 THz 2.05–4.30 THz	>90%
[56]	Unidirectional	broadband and narrowband Switchable	VO$_2$ (Phase Change) & Graphene (Fermi level)	No	0.75–1.15 THz 2.5-4.5 THz	>95% >90
This work	Bidirectional	Simultaneous broadband and narrowband	No external switch needed	Yes	1470-2290 nm 1550 nm	>90% 99.99%

REFERENCES

[1] N. Khalilazemi, M. Abdolrazzaghi, P. Musilek, and E. Baladi, "A planar compact absorber for microwave sensing based on transmission-line metamaterials," IEEE Sens. J., Vol. 24, no. 24, pp. 41864–41874, 2024.

[2] M.A. Khalil, W.H. Yong, M.S. Islam, L.Y. Chiong, A. Hoque, N. Ullah, H.H. GOH, T.A. KURNIAWAN, M.S. Soliman, and M.T. Islam, "Design of dual peak star shaped metamaterial absorber for S and C band sensing applications," Sci. Rep., Vol. 14, no. 1, pp. 26609(1-14), 2024.

[3] E. Eroglu and B. Chowdhury, Development of Multilayer Metamaterial Absorber for Medical Applications, 2024 International Conference on Electromagnetics in Advanced Applications (ICEAA). 2024.

[4] B. Salim and S. Maity, "A broadband metamaterial absorber for cloaking applications," in 2022 3rd International Conference for Emerging Technology (INCET), pp. 1–4, 2022.

[5] A. Armghan, J. Logeshwaran, S. Raja, K. Aliqab, M. Alsharari, and S.K. Patel, "Performance optimization of energy-efficient solar absorbers for thermal energy harvesting in modern industrial environments using a solar deep learning model," Heliyon, Vol. 10, no. 4, pp. e26371(1-19), 2024.

[6] Z. Qiu, G. Jin, and B. Tang, "Thermally controlled broadband Ge$_2$Sb$_2$Te$_5$-based metamaterial absorber for imaging

applications," Photonics, Vol. 11, pp. 272(1-9), Mar. 2024.

[7] G. Baffou and R. Quidant, "Thermo-plasmonics: using metallic nanostructures as nano-sources of heat," Laser Photon. Rev., Vol. 7, no. 2, pp. 171–187, Mar. 2013.

[8] A.F. Bukhanko, "Particular features of the optical properties of an anisotropic metamaterial with a near-zero dielectric permittivity," Opt. Spectrosc., Vol. 122, no. 4, pp. 661–669, 2017.

[9] A. Gazizov and M. Salakhov, "Tip-enhanced Raman scattering in epsilon-near-zero nanocavity," Opt. Spectrosc., Vol. 132, pp. 353–356, Sep. 2024.

[10] N. Kinsey and J. Khurgin, "Nonlinear epsilon-near-zero materials explained: opinion," Opt. Mater. Express, Vol. 9, no. 7, pp. 2793–2796, 2019.

[11] S.A. Schulz, A.A. Tahir, M.Z. Alam, J. Upham, I. De Leon, and R.W. Boyd, "Optical response of dipole antennas on an epsilon-near-zero substrate," Phys. Rev. A, Vol. 93, no. 6, pp. 063846(1-4), Jun. 2016.

[12] Z.T. Xie, J. Wu, H.Y. Fu, and Q. Li, "Tunable electro- and all-optical switch based on epsilon-near-zero metasurface," IEEE Photonics J., Vol. 12, no. 4, pp. 1–10, 2020.

[13] Y. Sha, Z.T. Xie, J. Wu, H.Y. Fu, and Q. Li, "All-optical switching in epsilon-near-zero asymmetric directional coupler," Sci. Rep., Vol. 12, no. 1, pp. 17958(1-10), 2022.

[14] X. Jiang, H. Lu, Q. Li, H. Zhou, S. Zhang, and H. Zhang, "Epsilon-near-zero medium for optical switches in a monolithic waveguide chip at 1.9 μm," Vol. 7, no. 11, pp. 1835–1843, 2018.

[15] Y. Vaddi, T.-L. Lim, M. Alam, S. Vangala, J. Upham, J. Hendrickson, and R. Boyd, "An Ultrafast all-optical switch with an epsilon-near-zero-based nanocavity," Advanced Photonics Congress 2024, paper NpTh3C.1, 2024.

[16] E. Li and A.X. Wang, "Femto-joule all-optical switching using epsilon-near-zero high-mobility conductive oxide," IEEE J. Sel. Top. Quantum Electron., Vol. 27, no. 2, pp. 1–9, 2021.

[17] Y. Wang, Z.T. Xie, Y. Sha, H.Y. Fu, and Q. Li, "Epsilon-near-zero based electro-optical and all-optical modulator for intensity and phase modulation," in 2023 Opto-Electronics and Communications Conference (OECC), pp. 1–3, 2023.

[18] A. Rafatmah, M. Miri, and N. Yasrebi, "Energy-efficient high-speed optical modulators based on the interplay of epsilon-near-zero effect in graphene and ITO," J. Opt. Soc. Am. B, Vol. 41, pp. 2048-2059, 2024.

[19] M.G. Wood, P.S. Finnegan, K.M. Musick, W.M. Mook, C.D. Nordquist, A.J. Grine, and D.K. Serkland, "Epsilon-near-zero modulators integrated on Si₃N₄ waveguides for Operation Shorter than 1 μm," in Frontiers in Optics and Laser Science 2023 (FiO, LS), Technical Digest Series. Tacoma, Washington: Optica Publishing Group, paper JTu4A.79, 2023.

[20] B. Zhou, E. Li, Y. Bo, and A.X. Wang, "High-speed plasmonic-silicon modulator driven by epsilon-near-zero conductive oxide," J. Light. Technol., Vol. 38, no. 13, pp. 3338–3345, 2020.

[21] M.G. Wood, S. Campione, S. Parameswaran, T.S. Luk, J.R. Wendt, D.K. Serkland, and G.A. Keeler, "Gigahertz speed operation of epsilon-near-zero silicon photonic modulators," Optica, Vol. 5, no. 3, pp. 233–236, 2018.

[22] Y. Kuang, Y. Liu, L. Tian, W. Han, and Z. Li, "A dual-slot electro-optic modulator based on an epsilon-near-zero oxide," IEEE Photonics J., Vol. 11, no. 4, pp. 1–12, 2019.

[23] E. Alvear-Cabezón, T. Taliercio, S. Blin, R. Smaali, F. Gonzalez-Posada, A. Baranov, R. Teissier, and E. Centeno, "Epsilon near-zero all-optical terahertz modulator," Appl. Phys. Lett., Vol. 117, no. 11, pp. 111101(1-5), Sep. 2020.

[24] A.R. Davoyan, A.M. Mahmoud, and N. Engheta, "Optical isolation with epsilon-near-zero metamaterials," Opt. Express, Vol. 21, no. 3, pp. 3279–3286, 2013.

[25] M. Vafaei, M. Moradi, and G.H. Bordbar, "Highly sensitive refractive index sensing by epsilon near zero metamaterials," Optik, Vol. 244, pp. 167617(1-11), 2021.

[26] H. Jiang, Y. Zhao, H. Ma, C. Feng, Y. Wu, W. Zhang, M. Chen, M. Wang, Y. Lian, Z. Cao, and J. Shao, "Polarization-independent, tunable, broadband perfect absorber based on semi-sphere patterned Epsilon-Near-Zero

films," Appl. Surf. Sci., Vol. 596, pp. 153551(1-9), 2022.

[27] S. Hayati Raad, M. Afshari-Bavil, and D. Liu, "Efficient and high-quality absorption enhancement using epsilon-near-zero cylindrical nano-shells constructed by graphene," Sci. Rep., Vol. 14, pp. 1-12 Mar. 2024.

[28] E.M. Smith, J. Chen, J.R. Hendrickson, J.W. Cleary, C. Dass, A.N. Reed, S. Vangala, and J. Guo., "Epsilon-near-zero thin-film metamaterials for wideband near-perfect light absorption," Opt. Mater. Express, Vol. 10, no. 10, pp. 2439–2446, 2020.

[29] L. Cheng, K. Huang, F. Wu, and X. Li, "Tunable nonlinear meta-absorber based on epsilon-near-zero metamaterial," J. Russ. Laser Res., Vol. 44, no. 2, pp. 148–155, 2023.

[30] H. Kondori, M. Ghadrdan, and M.A. Mansouri-Birjandi, "Bidirectional and broadband perfect absorber based on epsilon-near-zero material," Opt. Contin., Vol. 4, no. 4, pp. 745–755, 2025.

[31] Z. Meng, H. Cao, and X. Wu, "New design strategy for broadband perfect absorber by coupling effects between metamaterial and epsilon-near-zero mode," Opt. Mater., Vol. 96, pp. 109347(1-7), 2019.

[32] A. Corona, D. Murthy, and J.-L. Olvera-Cervantes, "Novel microwave filters based on Epsilon Near Zero waveguide tunnels," Microw. Opt. Technol. Lett., Vol. 53, pp. 1706-1710, Aug. 2011.

[33] H. Mu, C. Ding, T. Yi, Y. Wang, F. Meng, and J. Wang, "Tunable bandpass filter based on epsilon-near-zero metamaterials using liquid crystals," Liq. Cryst., Vol. 51, no. 5, pp. 773-782, Apr. 2024.

[34] J. Kyoung, D. Park, S. Byun, J. Lee, S. Choi, S. Park, and S. Hwang, "Epsilon-near-zero meta-lens for high resolution wide-field imaging," Opt. Express, Vol. 22, Dec. 2014.

[35] A. Anopchenko, L. Tao, C. Arndt, and H. (Ho W. Lee, "Field-effect tunable and broadband epsilon-near-zero perfect absorbers with deep subwavelength thickness," ACS Photonics, Vol. 5, pp. 2631-2637, Apr. 2018.

[36] J. Wu, M. Clementi, C. Huang, F. Ye, H. Fu, L. Lu, S. Zhang, Q. Li, and C.-S. Brès, "Thermo-optic epsilon-near-zero effects," Nat. Commun., Vol. 15, no. 1, pp. 794(1-9), 2024.

[37] Q. Wang, T. Liu, L. Li, C. Huang, J. Wang, M. Xiao, Y. Li, and W. Li, "Ultra-broadband directional thermal emission," Vol. 13, no. 5, pp. 793–801, 2024.

[38] I. Liberal and N. Engheta, "Manipulating thermal emission with spatially static fluctuating fields in arbitrarily shaped epsilon-near-zero bodies.," Proc. Natl. Acad. Sci. U. S. A., Vol. 115, no. 12, pp. 2878–2883, Mar. 2018.

[39] Z. Li, S. Butun, and K. Aydin, "Large-area, lithography-free super absorbers and color filters at visible frequencies using ultrathin metallic films," ACS Photonics, Vol. 2, no. 2, pp. 183–188, Feb. 2015.

[40] M. Yoo, H.K. Kim, and S. Lim, "Electromagnetic-based ethanol chemical sensor using metamaterial absorber," Sensors Actuators B Chem., Vol. 222, pp. 173–180, 2016.

[41] H. Zhou, D. Hu, G. Jia, J. Ji, X. Mu, X. Liu, and Z. Shang, "A novel chemical sensor using metamaterial absorber for methanol sensing aplications," The 7th International Multidisciplinary Conference on Optofluidics, pp. 1-2, 2017.

[42] C. Chen, L. Zhou, J. Yu, Y. Wang, S. Nie, S. Zhu, and J. Zhu, "Dual functional asymmetric plasmonic structures for solar water purification and pollution detection," Nano Energy, Vol. 51, pp. 451–456, 2018.

[43] S. Zhou, Z. Shen, R. Kang, S. Ge, and W. Hu, "Liquid crystal tunable dielectric metamaterial absorber in the terahertz range," Appl. Sci., Vol. 8, no. 11, pp. 1-7, 2018.

[44] H. Wang, Y. Yang, and L. Wang, "Switchable wavelength-selective and diffuse metamaterial absorber/emitter with a phase transition spacer layer," Appl. Phys. Lett., Vol. 105, no. 7, pp. 71907(1-5), Aug. 2014.

[45] Z. Song, A. Chen, and J. Zhang, "Terahertz switching between broadband absorption and narrowband absorption," Opt. Express, Vol. 28, pp. 2037-2044, Jan. 2020.

[46] Q. Wang, B. Li, L. Zeng, Q. Yang, X. Zhang, R. Wen, and C. Deng, "Switchable quadruple narrowband to broadband terahertz perfect absorber based on graphene and VO2 metamaterials," Diam. Relat. Mater., Vol. 142, pp. 110832(1-8), 2024.

[47] Y.-Y. Cheng, D. Meng, M.-Y. Xu, Y. Liu, P.-P. Zhuang, D. Lin, J. Liu, and Y.-S. Chen,, "Wide-band and narrow-band switchable terahertz absorber based on graphene," Results Phys., Vol. 52, pp. 106838(1-10), 2023.

[48] F. Wang, H. Gao, W. Peng, R. Li, S. Chu, L. Yu, and Q. Wang, "Bidirectional band-switchable nano-film absorber from narrowband to broadband," Opt. Express, Vol. 29, no. 4, pp. 5110–5120, 2021.

[49] S. Campione, I. Brener, and F. Marquier, "Theory of epsilon-near-zero modes in ultrathin films," Phys. Rev. B, Vol. 91, no. 12, pp. 121408(1-5), Mar. 2015.

[50] E. D. Palik, *Handbook of Optical Constants of Solids*. New York, 1998.

[51] L. Zhang, S. Love, A. Anopchenko, and H.W.H. Lee, "Hollow core optical fiber enabled by epsilon-near-zero material," Vol. 13, no. 7, pp. 1025–1031, 2024.

[52] Z. Wang, P. Zhou, and G. Zheng, "Electrically switchable highly efficient epsilon-near-zero metasurfaces absorber with broadband response," Results Phys., Vol. 14, pp. 102376(1-7), 2019.

[53] S.F.J. Blair, J.S. Male, S.A. Cavill, C.P. Reardon, and T.F. Krauss, "Photonic characterisation of Indium Tin Oxide as a function of deposition conditions," Nanomaterials, Vol. 13, no. 13, pp. 1-13, 2023.

[54] J. Wen, W. Sun, B. Liang, C. He, K. Xiong, Z. Wu, H. Zhang, H. Yu, Q. Wang, Y. Pan, Y. Zhang, and Z. Liu, "Dynamically switchable broadband–narrowband terahertz metamaterial absorber based on vanadium dioxide and multilayered structure," Opt. Commun., Vol. 545, pp. 129710(1-8), 2023.

[55] Y. Liu, R. Huang, and Z. Ouyang, "Terahertz absorber with dynamically switchable dual-broadband based on a hybrid metamaterial with vanadium dioxide and graphene," Opt. Express, Vol. 29, pp. 20839-20850, Jun. 2021.

[56] D. Gong, J. Mei, N. Li, and Y. Shi, "Tunable metamaterial absorber based on VO2-graphene," Mater. Res. Express, Vol. 9, no. 11, pp. 115803(1-10), 2022.

Hamideh Kondori was born in Zahedan, Iran in 1986. She received the BSc and MSc degrees in Electrical Engineering and telecommunication engineering in 2008 and 2012, respectively, from University of Sistan and Baluchestan, Iran.
She is currently a Ph.D. candidate at this university. In addition, she serves as a faculty member at Payame Noor University, Zahedan. Her research interests primarily focus on photonic crystals, optics, plasmonics, and metamaterials.

Majid Ghadrdan was born in Zabol in 1988. He received his Ph.D. in electrical engineering from the University of Sistan and Baluchestan, Iran in 2018. After completing his doctoral studies, he joined the University of Sistan and Baluchestan as an assistant professor, where he continues to contribute to the academic community. He has made significant contributions to the field, with a focus on nonlinear optics, plasmonics, and photonic crystals. As a respected professional in optics, Dr. Ghadrdan is actively involved in several professional societies, including the Optics and Photonics Society of Iran and the Iranian Society of Engineering Education. He has served as an editor for the International Journal of Industrial Electronics, Control, and Optimization (IECO), as well as a reviewer for numerous esteemed journals and conferences.

Mohammad Ali Mansouri-Birjandi was born in Birjand in 1961. He received his Ph.D. in electronic engineering from Tarbiat Modares University, Tehran, Iran in 2009. His major field of study is photonics. He has gained extensive work experience in photonic engineering. Currently, he holds the position of professor at the University of Sistan and Baluchestan. He has made significant contributions to the field, with a focus on plasmonics. Prof. Mansouri is also interested in photonics engineering and nanophotonics. As a respected professional in photonics, Prof. Mansouri-Birjandi is actively involved in several professional societies, including the Optics and Photonics Society of Iran, the Iranian Society of Engineering Education, and the Iranian Association of Electrical and Electronic Engineers (IAEEE). He has been recognized for his accomplishments and has received the top 2% most cited scientist in the world in 2022 to 2024.

THIS PAGE IS INTENTIONALLY LEFT BLANK.